TUDelft

Delft University of Technology

Transcriptomics and transposon mutagenesis identify multiple mechanisms of resistance to the FGFR inhibitor AZD4547

Kas, Sjors M.; De Ruiter, Julian R.; Schipper, Koen; Schut, Eva; Bombardelli, Lorenzo; Wientjens, Ellen; Drenth, Anne Paulien; De Korte-Grimmerink, Renske; Wessels, Lodewyk F.A.; More Authors

Important note
To cite this publication, please use the final published version (if applicable).
Please check the document version above.

Translational Science

Transcriptomics and Transposon Mutagenesis Identify Multiple Mechanisms of Resistance to the FGFR Inhibitor AZD4547

Sjors M. Kas[1,2], Julian R. de Ruiter[1,2,3], Koen Schipper[1,2], Eva Schut[1,2],
Lorenzo Bombardelli[2,4], Ellen Wientjens[1,2], Anne Paulien Drenth[1,2],
Renske de Korte-Grimmerink[1,2], Sunny Mahakena[5], Christopher Phillips[6],
Paul D. Smith[7], Sjoerd Klarenbeek[8], Koen van de Wetering[4], Anton Berns[2,4],
Lodewyk F.A. Wessels[2,3,9], and Jos Jonkers[1,2]

Abstract

In human cancers, FGFR signaling is frequently hyperactivated by deregulation of FGF ligands or by activating mutations in the FGFR receptors such as gene amplifications, point mutations, and gene fusions. As such, FGFR inhibitors are considered an attractive therapeutic strategy for patients with mutations in FGFR family members. We previously identified *Fgfr2* as a key driver of invasive lobular carcinoma (ILC) in an *in vivo* insertional mutagenesis screen using the *Sleeping Beauty* transposon system. Here we explore whether these FGFR-driven ILCs are sensitive to the FGFR inhibitor AZD4547 and use transposon mutagenesis in these tumors to identify potential mechanisms of resistance to therapy. Combined with RNA sequencing-based analyses of AZD4547-resistant tumors, our *in vivo* approach identified several known and novel potential resistance mechanisms to FGFR inhibition, most of which converged on reactivation of the canonical MAPK–ERK signaling cascade. Observed resistance mechanisms included mutations in the tyrosine kinase domain of FGFR2, overexpression of MET, inactivation of RASA1, and activation of the drug-efflux transporter ABCG2. ABCG2 and RASA1 were identified only from *de novo* transposon insertions acquired during AZD4547 treatment, demonstrating that insertional mutagenesis in mice is an effective tool for identifying potential mechanisms of resistance to targeted cancer therapies.

Significance: These findings demonstrate that a combined approach of transcriptomics and insertional mutagenesis *in vivo* is an effective method for identifying potential targets to overcome resistance to therapy in the clinic. *Cancer Res; 78(19); 5668–79. ©2018 AACR.*

Introduction

FGFRs are members of the receptor tyrosine kinase (RTK) family that bind to different FGF family members and are upstream of both the MAPK–ERK and PI3K–AKT signaling pathways. FGFRs dimerize upon FGF ligand binding, which results in cross-phosphorylation of the receptors cognate kinase domains and allows the binding of the adaptor protein FGFR substrate 2α (FRS2α), a key transducer of FGFR signaling (1). Once bound, subsequent phosphorylation of FRS2α induces the recruitment of growth factor receptor-bound 2 (GRB2) and son of sevenless (SOS), resulting in activation of the MAPK–ERK signaling pathway. In contrast, activation of the PI3K–AKT signaling pathway is mediated by interactions between the FRS2α complex and GRB2-associated binding protein 1 (GAB1; ref. 1).

In human cancers, FGFR signaling is frequently hyperactivated by deregulation of FGF ligands or by activating mutations in the receptors, which predominantly consist of gene amplifications, point mutations, and gene fusions (2, 3). As such, FGFR inhibitors are considered to be an attractive therapeutic strategy for patients with mutations in FGFR family members. Currently, no FGFR-targeted therapies are approved for the treatment of human cancer, but multiple therapeutics targeting FGFR signaling are under investigation in several phase I/II clinical trials in different types of cancer (2, 3). These encompass several different approaches for inhibiting FGFR, including nonselective and selective FGFR small-molecule tyrosine kinase inhibitors, monoclonal antibodies against FGFRs and FGF ligand traps.

Although these initial trials have shown promising results concerning tolerability and antitumor activity of several FGFR inhibitors in a subset of patients (2, 4–9), more research is

[1]Division of Molecular Pathology, The Netherlands Cancer Institute, Amsterdam, the Netherlands. [2]Oncode Institute, Amsterdam, The Netherlands. [3]Division of Molecular Carcinogenesis, The Netherlands Cancer Institute, Amsterdam, the Netherlands. [4]Division of Molecular Genetics, The Netherlands Cancer Institute, Amsterdam, the Netherlands. [5]Division of Molecular Oncology, The Netherlands Cancer Institute, Amsterdam, the Netherlands. [6]Discovery Sciences, IMED Biotech Unit, AstraZeneca, Cambridge, United Kingdom. [7]Bioscience, Oncology, IMED Biotech Unit, AstraZeneca, Cambridge, United Kingdom. [8]Experimental Animal Pathology, The Netherlands Cancer Institute, Amsterdam, the Netherlands. [9]Department of EEMCS, Delft University of Technology, Delft, the Netherlands.

S.M. Kas and J.R. de Ruiter contributed equally to this article.

Current address for K. van de Wetering: Department of Dermatology & Cutaneous Biology, Sidney Kimmel Medical College, Philadelphia.

Corresponding Authors: Jos Jonkers, The Netherlands Cancer Institute, Plesmanlaan 121, Amsterdam, 1066CX, the Netherlands. Phone: 31-205122000; Fax: 31-205122050; E-mail: j.jonkers@nki.nl; and Lodewyk F.A. Wessels, Phone: 31-205127987; E-mail: l.wessels@nki.nl

AACR

required to determine the right criteria for patient selection and to tackle potential resistance mechanisms to improve FGFR-targeted therapies. Several studies have already identified resistance mechanisms to FGFR-targeting agents, including polyclonal secondary FGFR mutations (including gatekeeper mutations; refs. 10–12), activation of alternative RTKs (13–16), and paracrine signaling of the tumor stroma (17, 18). However, because most of these mechanisms are identified in *in vitro* studies, they may not encompass the complete spectrum of resistance mechanisms to FGFR inhibitors.

In a previous study, we identified *Fgfr2* as a key driver of invasive lobular breast carcinoma (ILC) using a *Sleeping Beauty* (*SB*)-based transposon insertional mutagenesis screen in mice (19). In this work, we explore how mouse ILCs (mILC) with *SB* transposon insertions in *Fgfr2* respond to treatment with the selective FGFR inhibitor AZD4547, and by which mechanisms they acquire resistance to FGFR inhibition. Our results show that the tumors exhibit increased FGFR signaling and initially regress upon treatment with AZD4547, but eventually develop treatment resistance. By performing a multiomics analysis focusing on the resistant tumors, we identify several known and novel mechanisms by which tumors become resistant to AZD4547 treatment. Two of these mechanisms were uniquely identified from *de novo* transposon insertions that were acquired during treatment, demonstrating that insertional mutagenesis in mice is an effective tool for identifying resistance mechanisms to targeted cancer therapies.

Materials and Methods

Orthotopic transplantations and AZD4547 intervention

Orthotopic transplantations of small tumor fragments were performed as previously described by Doornebal and colleagues (20). For the WESB-*Fgfr2* tumor-derived cells, 200,000 cells were injected orthotopically into the right fat pad of 8- to 15-week-old wild-type syngeneic recipient FVB females in 20 µL Matrigel (Corning) and PBS (1:1). For the WESB-*Fgfr2*-EV and WESB-*Fgfr2*-ABCG2 cells, 200,000 cells were injected orthotopically into the right fat pad of 8-week-old NMRI-nude females (Janvier Labs) in 20 µL Matrigel (Corning) and PBS (1:1). All the drug interventions were initiated as soon as the mammary tumors reached a size of 5×5 mm (62.5 mm^3; tumor volume: length $\times$ width^2 $\times$ 0.5). The treatments were performed daily by oral gavage for the indicated time with either the vehicle (1%-Tween-80 in demineralized water) or AZD4547 (AstraZeneca) at a dose of 12.5 mg/kg/day. The experimental cohort was monitored and mice were sacrificed (overall survival) when the (total) mammary tumor burden reached a size of approximately 1500 mm^3 (tumor volume: length $\times$ width^2 $\times$ 0.5) or suffered from clinical signs of distress (respiratory distress, ascites, distended abdomen, rapid weight loss, and severe anemia) caused by mammary tumor burden or metastatic disease. One hour after the last dosing, mice were sacrificed and the tumor, lungs, liver, spleen, and tumor-draining lymph nodes were collected for further analysis. The mouse technicians were blinded to the sample groups for the treatments of WESB-*Fgfr2* and WESB-*Fgfr2*-ABCG2 established tumors in mice. All animal experiments were approved by the Animal Ethics Committee of the Netherlands Cancer Institute and performed in accordance with institutional, national and European guidelines for Animal Care and Use.

Cell culture

The isolation of primary tumor cells of the *SB*-induced mILCs (referred to as WESB cells) was performed as previously described by Kas and colleagues (19). WESB cells were cultured in DMEM-F12 medium containing 10% FBS, 100 IU/mL penicillin, 100 µg/mL streptomycin (all from Life Technologies). MEF3.8 cells were cultured in DMEM-F12 medium containing 10% FBS, 100 IU/mL penicillin, 100 µg/mL streptomycin (all from Life Technologies). Phoenix packaging cells were cultured in Iscove's medium (Life Technologies) containing 10% FBS, 100 IU/mL penicillin, and 100 µg/mL streptomycin. WESB-*Fgfr2* cells were transduced with LZRS-IRES-GFP or LZRS-*Bcrp1*-IRES-GFP as previously described by Allen and colleagues (21). Single GFP$^+$ cells were sorted and allowed to recover before they were used in the experiments. Cell authentication was not conducted. All cell lines were kept at low passage and routinely tested for *Mycoplasma* contamination using the MycoAlert Mycoplasma Detection Kit (Lonza).

Additional experimental details regarding the cell viability, clonogenic, and competition assays are described in the Supplementary Data.

Vesicular transport assays

Vesicular transport assays were performed using the rapid filtration method as previously described (22, 23). Additional experimental details are described in the Supplementary Data.

Nucleic acid isolation

DNA and RNA were isolated from whole tumor pieces using the Allprep DNA/RNA Mini Kit (Qiagen) according to the manufacturer's protocol.

Additional experimental details regarding the detection of the endogenous *Fgfr2–Tbc1d1* fusion and the *Met* qPCR copy number analysis are described in the Supplementary Data.

Analysis of *SB* transposon insertions

Transposon insertions were amplified and mapped following a previously described tagmentation-based DNA sequencing protocol (24). Additional experimental details and the analysis of the insertions sites are described in the Supplementary Data.

Antibodies

The primary antibodies to the following proteins were used: FGFR2 (1:1,000, GeneTex 10648), phospho-FGFR (1:1,000, CST 3471), FRS2 (1:1,000, ProteinTech 11503-1-AP), phospho-FRS2 (Tyr436) (1:1,000, Abcam 193363), AKT1 (1:1000, CST 2938), phospho-AKT(Ser473; 1:1,000, CST 4060), p44/42 MAP kinase (1:1,000, CST 4695), phospho-p44/42 MAPK ERK1/ERK2 (Thr202/Tyr204; 1:1,000 CST 9101), ABCG2 (1:400, Abcam 24115) and β-actin (1:50,000, Sigma A5441).

Additional details regarding immunoblotting and IHC are described in the Supplementary Data.

In silico modeling of the FGFR2 kinase in complex with the inhibitor AZD4547

A composite complex of AZD4547 bound to mutated FGFR2 was built using the crystal structure of the FGFR1 kinase domain in complex with AZD4547 (PDB code V405) as a template. A structural alignment of the FGFR2 kinase domain crystal structure (PDB code 2PVF) was performed and the positions of the resistance mutations were mapped onto this alignment. Molecular graphic images were prepared using the CHIMERA package (25).

Statistical analysis

For the mouse studies, no statistical tests were performed to determine the appropriate sample size. Survival probabilities were estimated using the Kaplan–Meier method and compared using the Mantel–Cox test. The effect of AZD4547 treatment on tumor growth of WESB-*Fgfr2*-EV and WESB-*Fgfr2*-ABCG2 established tumors was tested using mixed linear models (details in Supplementary Data). To test for differential expression of *Abcg2*, *Rasa1*, and *Pcdh15* over the insertion sites across all *SB*-induced tumors, we used the group-wise differential expression test implemented in IM-Fusion (26). The investigators were not blinded to the sample groups for all experiments. Graphs and error bars represent mean ± SD. Python 3.5, R 3.3.1 and GraphPad Prism 7.03 were used for the statistical analyses. *P* values < 0.05 were considered significant.

Data availability

Raw tagmentation and RNA-sequencing data are available in ENA under accession number PRJEB25507.

Results

Activation of *Fgfr2* induces mILC formation

In a previous study, we performed a *SB* insertional mutagenesis screen in mice with mammary-specific inactivation of *Cdh1* (encoding E-cadherin) to identify genes and pathways driving the development of ILC (19). Analysis of common insertion sites (CIS) in the *SB*-induced mILCs showed that a majority (56 of 99) of these tumors had *SB* insertions in *Fgfr2*, providing strong evidence that *Fgfr2* is a driver of ILC.

To confirm active FGFR signaling in mILCs with *SB* insertions in *Fgfr2*, we established cell lines from two *SB*-induced tumors, one with an insertion upstream of *Fgfr2* (WESB-*Fgfr2*) and one without an insertion in or near *Fgfr2* (WESB). We next compared the expression of FGFR2 and downstream signaling proteins between the two tumor cell lines. Although immunoblot analysis with an anti-FGFR2 antibody revealed no expression of native FGFR2 in either of the cell lines, we observed a doublet of approximately 240 kDa that was only expressed in the WESB-*Fgfr2* cell line (Fig. 1a). This size coincided with the predicted protein size of a gene fusion between *Fgfr2* and *Tbc1d1* (Supplementary Fig. S1A and S1B), which we previously identified in RNAseq data from this *SB*-induced mILC (26). Similar FGFR2 gene fusions were previously identified in several other studies, which demonstrated that these fusions result in increased FGFR signaling (27). In line with this, comparison of signaling proteins downstream of FGFR2 showed increased expression of phosphorylated FRS2α in WESB-*Fgfr2* tumor-derived cells compared with WESB cells.

These results demonstrate that WESB-*Fgfr2* cells show increased expression of an *Fgfr2*–*Tbc1d1* fusion gene, which is driven by an *SB* insertion upstream of *Fgfr2*. The increased expression of this fusion gene results in activation of FGFR signaling, suggesting that FGFR inhibition could be an interesting therapeutic strategy in these tumors.

Mouse ILCs with *SB* insertions in *Fgfr2* are dependent on FGFR signaling

To determine if WESB-*Fgfr2* cells were indeed sensitive to FGFR inhibition, we treated these cells with the selective FGFR inhibitor AZD4547, which is currently being evaluated in several early-phase clinical trials (2). After treatment with 100 nmol/L AZD4547, WESB-*Fgfr2* cells showed a decrease in expression of phosphorylated FGFR, FRS2α, and ERK1/2 (Fig. 1b), confirming inhibition of the FGFR signaling pathway. Compared with WESB cells, the WESB-*Fgfr2* cells also showed reduced viability upon exposure to increasing concentrations of AZD4547 (Supplementary Fig. S1C), indicating that WESB-*Fgfr2* cells are dependent on FGFR signaling for their survival *in vitro*.

To determine the efficacy of AZD4547 *in vivo*, we orthotopically transplanted WESB-*Fgfr2* tumor fragments into multiple wild-type syngeneic recipient FVB animals and treated these animals with vehicle or AZD4547 (12.5 mg/kg/day) daily via oral gavage (Fig. 1C). To reduce the potential toxicity of prolonged treatment and to test the effect of a "drug holiday" on tumor growth, the animals were treated using either a continuous or an intermittent dosing schedule (Supplementary Fig. S1D). In both dosing schedules, tumors treated with AZD4547 showed decreased expression of downstream FGFR signaling and increased expression of cleaved caspase-3 (Supplementary Fig. S1E–S1G), which resulted in tumor regression within 10 to 20 days after start of the treatment (Fig. 1D and E). Furthermore, the majority of the AZD4547-treated tumors (9 of 10 continuous-treated and 13 of 14 intermittent-treated tumors) did not show any regrowth within the first treatment cycle of 24 days.

In the majority of mice, continuous treatment with AZD4547 resulted in tumor control for at least 40 days after start of the treatment, resulting in an increased overall survival compared with the vehicle-treated animals (Fig. 1F). Notably, 2 of 10 sacrificed animals did not show any remaining tumor cells. In contrast, all intermittently treated mice showed tumor regrowth after the first treatment cycle of 24 days. However, these tumors remained sensitive to multiple additional cycles of AZD4547 treatment (Supplementary Fig. S2A), resulting in an increased overall survival compared with the vehicle-treated animals (Fig. 1G). Similar results were obtained with continuous AZD4547 treatment of mice after the orthotopic injection of WESB-*Fgfr2* tumor-derived cells (Supplementary Fig. S2B and S2C).

Although the overall survival of AZD4547-treated mice was increased compared with vehicle-treated animals, there was no significant difference in survival between the continuous dosing (107 days) and the intermittent dosing (126 days) groups. However, in the continuous dosing group an increased number of animals succumbed due to clinical signs of distress (respiratory distress, ascites, distended abdomen, rapid weight loss, and severe anemia), suggesting that the intermittent treatment schedule is less toxic for the animals (Supplementary Fig. S2D). In spite of the potent anticancer activity of AZD4547, both treatment schedules failed to deliver long-term tumor control, most likely due to the emergence of acquired therapy resistance. This reflects the major problem observed in patients with cancer treated with targeted anticancer therapies.

Transcriptome analysis identifies known and novel secondary FGFR2 mutations and increased MET expression in AZD4547-resistant tumors

To explore potential resistance mechanisms to FGFR inhibition, we performed RNA-sequencing of AZD4547-sensitive and -resistant tumors obtained from vehicle-treated and AZD4547-treated animals (Supplementary Table S1), respectively, and

compared their mutational spectra to identify mutations that were acquired during AZD4547 treatment. In this approach, we initially focused on known resistance mechanisms to FGFR-targeting therapeutics (10–16), which include upregulation of alternative RTKs and secondary FGFR mutations.

To assess if upregulation of other RTKs could explain the resistance of these tumors, we used RNA-sequencing data to determine changes in gene expression for *Kit*, *Met*, and all FGFR-, EGFR-, and IGF-related RTKs. For this purpose, we used DIDS, an algorithm that is specifically designed to identify
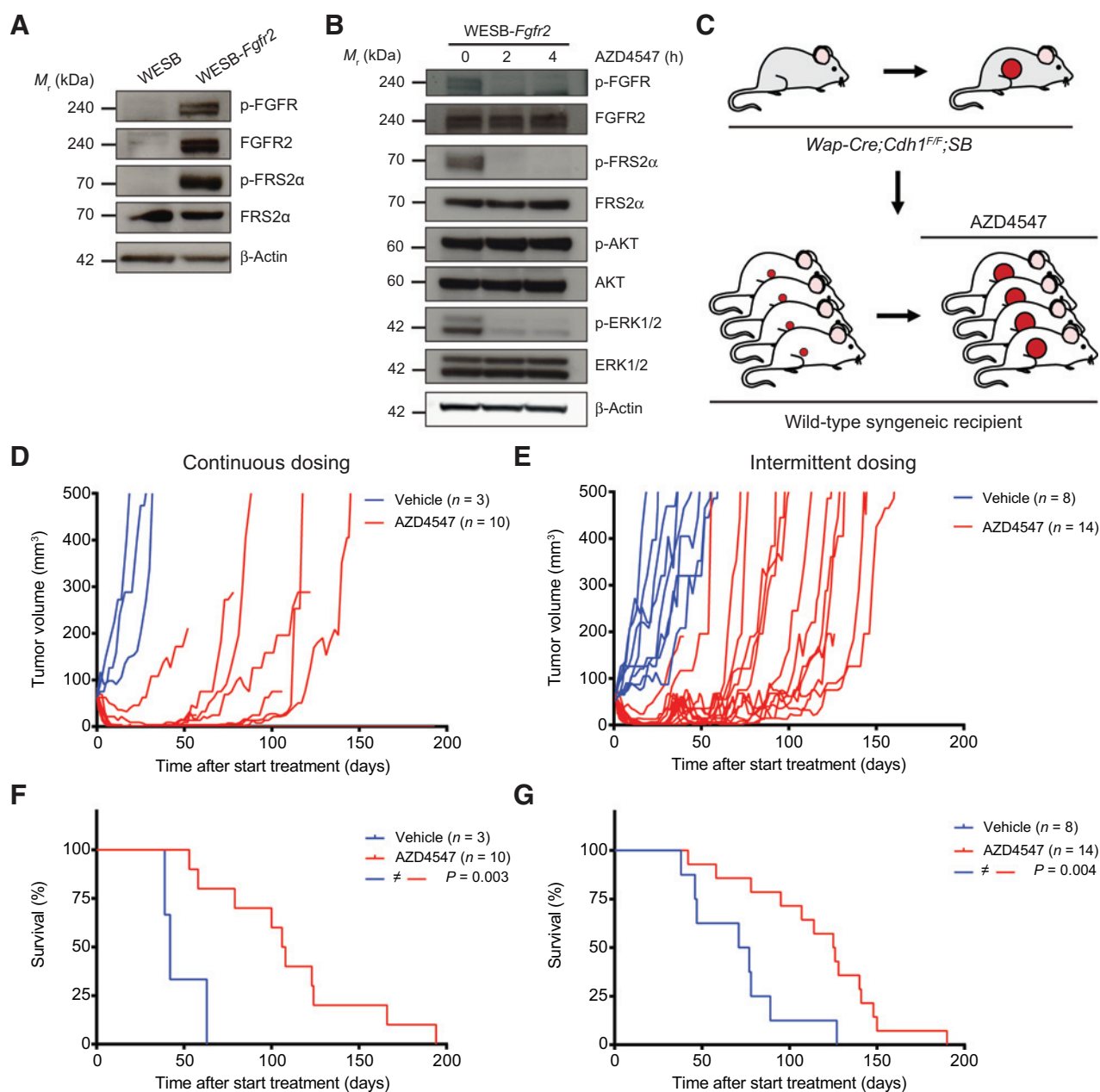

Figure 1.
Intervention study with AZD4547 in mILCs with active FGFR signaling. **A,** Representative immunoblot ($n = 3$) for the expression of FGFR2 and its downstream signaling proteins in WESB and WESB-*Fgfr2* cells. β-Actin was used as a loading control. **B,** The effect of FGFR inhibition on FGFR signaling in WESB-*Fgfr2* cells after short-term treatment with the FGFR inhibitor AZD4547 (100 nmol/L), as visualized by immunoblotting with antibodies detecting total and phosphorylated FGFR, FRS2α, AKT, and ERK1/2. β-Actin was used as a loading control. **C,** Schematic overview depicting the orthotopic transplantation of *SB*-induced mILC fragments into wild-type syngeneic recipient mice and the subsequent drug intervention with AZD4547. **D** and **E,** Tumor growth kinetics of orthotopically transplanted WESB-*Fgfr2* tumors under the continuous (**D**) and intermittent (**E**) treatment schedules with vehicle (blue) or AZD4547 (red). **F** and **G,** Kaplan–Meier curves showing the overall survival of tumor-bearing mice under continuous (**F**) and intermittent (**G**) treatment with vehicle (blue) or AZD4547 (red). P values were calculated using a Mantel–Cox test.

Kas et al.

differentially expressed genes in heterogeneous populations (28). Although this analysis did not identify any RTKs that were significantly differentially expressed across multiple samples, it did identify two AZD4547-resistant tumors with increased expression of *Met* [also known as hepatocyte growth factor receptor (HGFR)] and one AZD4547-resistant tumor with increased expression of insulin-like growth factor 1 receptor (*Igf1r*), compared with vehicle-treated tumors (Fig. 2A; Supplementary Fig. S3A). Subsequent analysis of IGF1R and MET protein expression by IHC did not support IGF1R as a potential resistance mechanism, because no correlation was observed between expression levels of *Igf1r* mRNA and IGF1R protein (Fig. 2B). In contrast, both AZD4547-resistant tumors with high *Met* mRNA expression showed amplification of *Met* (Supplementary Fig. S3B) and overexpression of MET protein (Fig. 2C), whereas vehicle-, AZD4547-treated, and other AZD4547-resistant tumors were negative for MET expression (Supplementary Fig. S3C). These *in vivo* results are in line with previous *in vitro* studies showing that upregulation of MET attenuates the efficacy of FGFR inhibition in tumor cells

(14, 15), indicating that upregulation of MET may also counteract the therapeutic efficacy of AZD4547 *in vivo*. In contrast to previous *in vitro* studies (13, 16), we did not observe an obvious increase in mRNA expression of the *Egfr* or other EGFR-family members in any of the AZD4547-resistant tumors.

Next, to determine if any mutations in RTKs or members of the MAPK–ERK pathway could explain the resistance of these tumors, we used the RNA-sequencing data to identify mutations in the above-mentioned RTKs and genes involved in the MAPK–ERK signaling pathway (Supplementary Table S2). Using this approach, we identified 12 missense mutations in *Fgfr2* affecting 11 different amino acids, of which four were located in the third immunoglobulin (Ig)-like domain (IgIII) and seven were located in the tyrosine kinase domain (Fig. 2D).

To predict the effects of the mutations in the FGFR2 kinase domain on AZD4547 binding, we mapped the seven missense mutations onto the FGFR2 protein structure and observed that residues I567, N568, V581, E584, S587 reside in the ATP-binding pocket of FGFR2 (Fig. 2E). As a consequence, these mutated
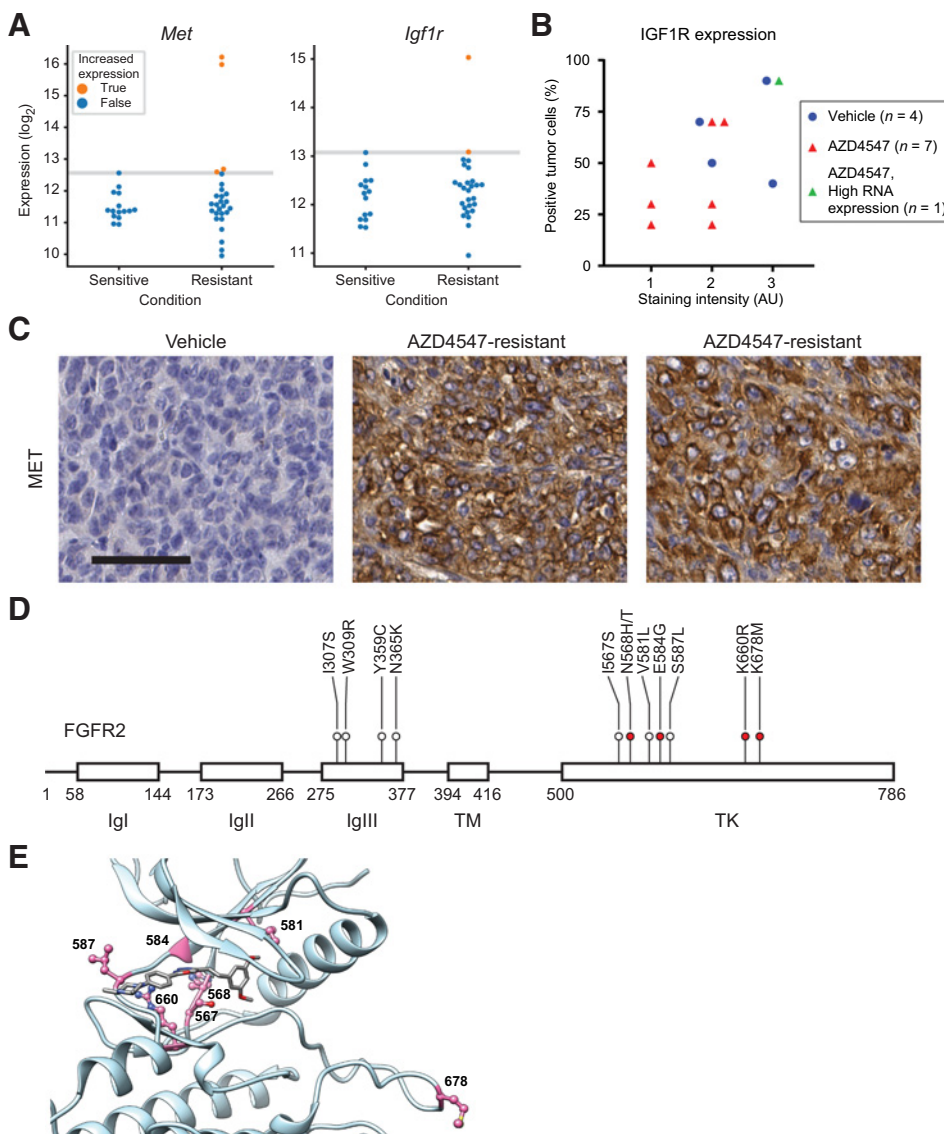

Figure 2.
Transcriptome analysis of AZD4547-resistant tumors. **A,** Differential expression analysis of *Met* and *Igf1r* in AZD4547-sensitive ($n = 15$) and -resistant ($n = 27$) tumors using DIDS, showing outliers for *Met* ($n = 2$) and *Igf1r* ($n = 1$). **B,** Quantification of IGF1R expression in AZD4547-sensitive ($n = 4$) and -resistant ($n = 8$) tumors. AU, arbitrary unit. **C,** Representative immunohistochemical stainings of MET in AZD4547-sensitive (vehicle) and -resistant tumors. Scale bar, 50 μm. **D,** Schematic overview showing the locations of mutations identified for *Fgfr2* in the AZD4547-resistant tumors. Red mutations have been previously reported in patients with *FGFR2* fusion–positive cholangiocarcinoma, whose tumors acquired resistance to the selective FGFR inhibitor NVP-BGJ398. Numbers indicate amino acid residue positions (mouse). Ig, immunoglobulin-like domain; TM, transmembrane domain; TK, tyrosine kinase domain. **E,** *In silico* modeling of AZD4547 (middle) in the ATP-binding pocket of FGFR2. The FGFR2 kinase domain is depicted as a sky-blue ribbon with residues of interest colored by atom type: carbon, pink; nitrogen, blue; oxygen, red. AZD4547 is colored by atom type: carbon, gray; nitrogen, blue; oxygen, red.

residues directly perturb the binding site of AZD4547. In addition, the E584G mutation is located in the kinase hinge and introduces flexibility at the key recognition motif for AZD4547. The K660R mutation is adjacent to the binding site, which suggests that the binding of AZD4547 is indirectly perturbed. Finally, the K678M mutation is located in the kinase activation loop, suggesting that this mutation alters the dynamics of the activation loop and favors the active conformation.

Interestingly, four out of the seven missense mutations in the tyrosine kinase domain reflected recurrent point mutations that were previously reported in patients with *FGFR2* fusion–positive cholangiocarcinoma, whose tumors acquired resistance to the selective FGFR inhibitor NVP-BGJ398 (10). In this previous work, structural characterization combined with functional *in vitro* studies showed that these FGFR2 kinase mutations either induce a steric clash with NVP-BGJ398 in the ATP-binding pocket or destabilize the inactive conformation of the kinase. Together, these data indicate that the seven mutations in the ATP-binding pocket of FGFR2 disrupt the binding of selective FGFR tyrosine kinase inhibitors and therefore hamper their therapeutic efficacy.

AZD4547-resistant *SB*-induced tumors show *de novo* insertions in candidate resistance genes

Because of the presence of a constitutively active *SB* transposase, the *SB*-induced mILCs could be capable of developing resistance by acquiring *de novo* transposon insertions in or near resistance genes during AZD4547 treatment. To determine if *SB*-mediated mutagenesis might indeed be driving resistance in some of these tumors, we performed an insertion analysis of 27 AZD4547-resistant *SB*-induced tumors and compared the identified *SB* insertions to those found in the donor tumor and 15 vehicle-treated tumors. Globally, this analysis showed that the majority of the clonal insertions in the donor tumor (e.g., *Fgfr2*, *Ppp1r12a*, *Slc16a9*, and *Trps1*) were maintained after orthotopic transplantation and long-term treatment of the tumor-bearing mice (Supplementary Fig. S4A; Supplementary Tables S1 and S3). Interestingly, additional *SB* insertions were observed in both vehicle- and AZD4547-treated tumors, indicating that mobilization of transposons still occurs after transplantation of *SB*-induced tumors.

To specifically identify *de novo* insertions that might be driving resistance to AZD4547, we filtered for genes that contained *SB* insertions in the AZD4547-resistant tumors but not in the donor or vehicle-treated tumors (Supplementary Fig. S4B). This analysis revealed three candidate resistance genes (*Abcg2*, *Rasa1*, and *Pcdh15*) with insertions in at least three AZD4547-resistant tumors (Fig. 3A). Of these three genes, *Abcg2* contained several independent insertions that were mainly in the sense orientation and located upstream of the transcription start site (Fig. 3B), indicating that these insertions result in increased *Abcg2* expression. In support of this, these insertions coincided with increased mRNA and protein expression of ABCG2 (Fig. 3C; Supplementary Fig. S5A–S5C). Variable ABCG2 expression highlights intratumor heterogeneity in mechanisms of AZD4547 resistance. In contrast to *Abcg2*, *Rasa1*, and *Pcdh15* contained either a mix of sense/antisense insertions or purely antisense insertions, suggesting that these genes are inactivated (Fig. 3D–G). Further analysis revealed decreased expression of exons downstream of the insertion sites in *Rasa1*, supporting inactivation of *Rasa1* via truncation of the gene, whereas expression of *Pcdh15* was not markedly affected.

To investigate whether insertions from the donor tumor might contribute to intrinsic treatment resistance, we compared the relative support scores of insertions between untreated tumors (vehicle-treated tumors and the donor tumor) and AZD4547-resistant tumors to determine if insertions in specific genes were enriched after AZD4547 treatment. This analysis identified six genes (*Arid1a*, *Myh9*, *Fbxw7*, *Matr3*, *Slc16a9*, and *Map4k4*) with increased support scores in AZD4547-resistant tumors, indicating that subclones with insertions in these genes are selected for during treatment (Supplementary Fig. S5D). These genes might therefore be involved in intrinsic resistance to AZD4547. Interestingly, the top three genes (*Arid1a*, *Myh9*, and *Fbxw7*) were previously identified as candidate driver genes in ILC formation (19).

Collectively, these results show that persistent mobilization of transposons in *SB*-induced mILCs allows them to acquire new insertions during treatment and that this approach can be used to identify novel resistance mechanisms. Our analysis implicates upregulation of *Abcg2* and inactivation of *Rasa1* as additional resistance mechanisms to AZD4547, which were not previously identified with our mutational analyses. This demonstrates that combining insertional mutagenesis with drug treatments poses an effective strategy for identifying resistance mechanisms to targeted therapies in mice.

Loss of RASA1 reduces sensitivity of WESB-*Fgfr2* tumor cells to AZD4547

To test whether inactivation of *Rasa1* induces resistance to AZD4547 treatment, we transfected WESB-*Fgfr2* tumor-derived cells with modified pX330 vectors containing single guide RNAs (sgRNA) targeting three different genomic regions of *Rasa1* or a nontargeting sgRNA (sgNT). All the *Rasa1* targeting sgRNAs induced efficient modification of the *Rasa1* target sites in the transfected cell populations (Supplementary Fig. S5E–S5G), as determined by tracking of insertions or deletions [indels] by decomposition (TIDE) analysis (29). To test for drug sensitivity, we performed an *in vitro* competition assay with a mixture of WESB-*Fgfr2*-sgNT and WESB-*Fgfr2*-sg*Rasa1* cells (1:1 ratio) in the presence or absence of 2 μmol/L AZD4547 and subsequently quantified the allele distribution of the polyclonal population using the frequency of frameshift mutations in *Rasa1* (Fig. 3H). After prolonged AZD4547 treatment, the polyclonal population was enriched for *Rasa1* frameshift mutations for all three *Rasa1*-targeted regions (Fig. 3I), indicating that *Rasa1*-depleted cells were less sensitive to AZD4547 treatment compared with control cells. In contrast, the allele distributions were not affected when cells were cultured without AZD4547, demonstrating that the observed effect was not due to a difference in proliferation between WESB-*Fgfr2*-sgNT and WESB-*Fgfr2*-sg*Rasa1* cells. Altogether, these data show that inactivation of *Rasa1* reduces the sensitivity of WESB-*Fgfr2* cells to AZD4547 treatment.

AZD4547 is a substrate of ABCG2

Abcg2 is an ATP-binding cassette (ABC) efflux transporter, suggesting that overexpression of this gene may induce resistance through increased extrusion of AZD4547 from the tumor cells. To determine if this is indeed the case, we first sought to confirm that AZD4547 is a substrate for the ABCG2 transporter. To this end, we performed a vesicular transport assay (Fig. 4a), in which we measured the uptake of tritium-labeled methotrexate ([^{3}H]-MTX) in inside-out Sf9-membrane vesicles expressing ABCG2

(Sf9-ABCG2), both in the presence and absence of increasing concentrations of AZD4547, and compared the results to the uptake of [³H]-MTX in control Sf9-membrane vesicles (Sf9-control). This showed that ATP-dependent uptake of [³H]-MTX by ABCG2 was inhibited by AZD4547 (Fig. 4b), indicating that AZD4547 is indeed a substrate of ABCG2.

Overexpression of ABCG2 reduces sensitivity to AZD4547

To further explore whether increased expression of *Abcg2* reduces the sensitivity of cells to AZD4547, we used mouse embryonic fibroblasts (MEF) derived from *Abcb1a⁻/⁻*; *Abcb1b⁻/⁻*;*Abcc1⁻/⁻* mice (hereafter referred to as MEF3.8), which have very low background expression of endogenous
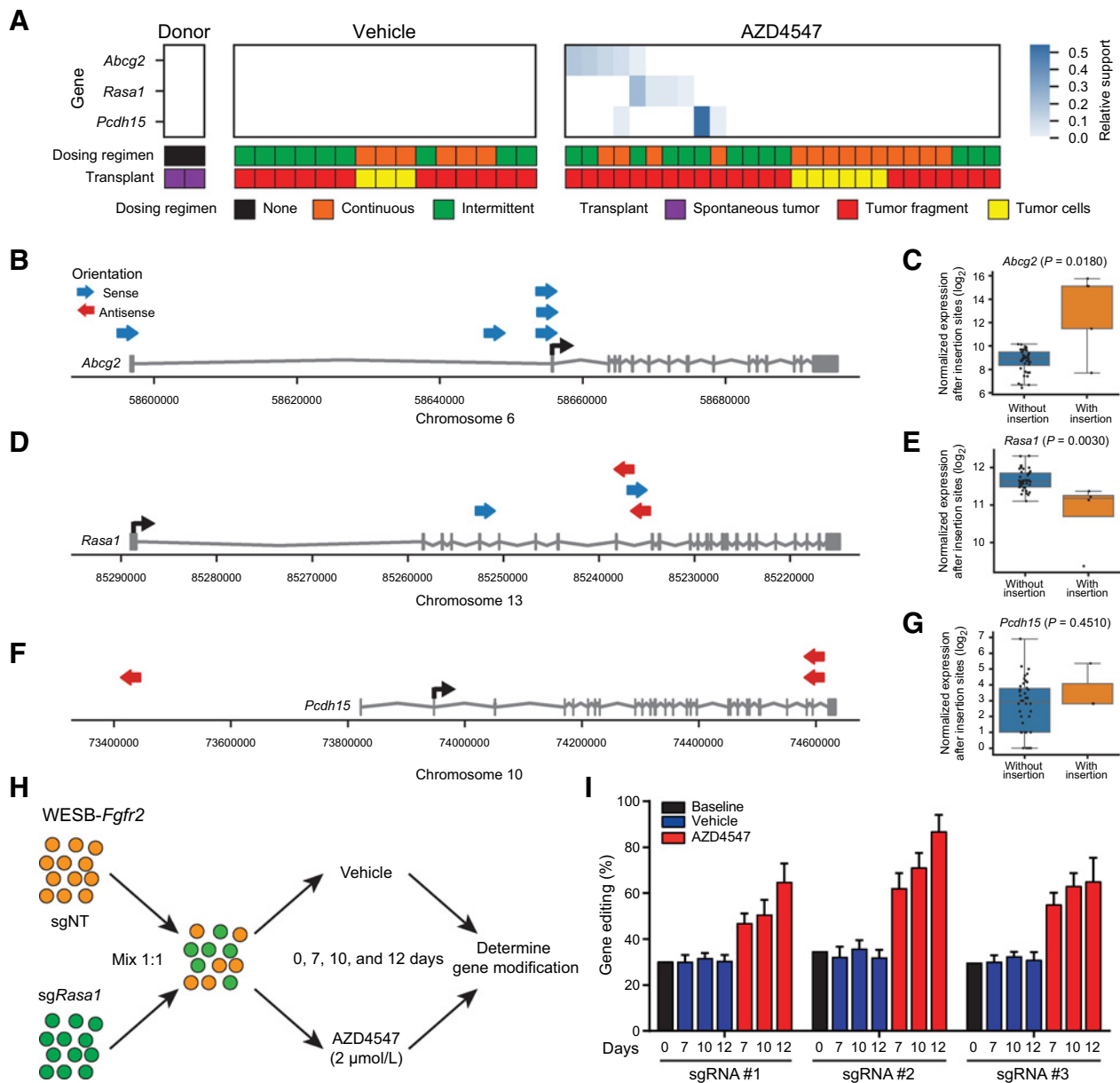
Figure 3.
Overview of insertions and corresponding gene expression of candidate resistance genes. **A,** Overview of insertions in candidate resistance genes that were mutated in at least three AZD4547-resistant tumors (*n* = 27) and were not mutated in any of the donor (two technical replicates) or vehicle-treated (*n* = 15) tumors. Relative clonality of insertions is indicated by "relative support" scores (blue), which were calculated by counting the number of mate pairs supporting an insertion and normalizing these "support" scores to the highest score of the corresponding sample. **B–G,** Left, visualization of *SB* insertions (arrows) in *Abcg2* (**B**), *Rasa1* (**D**), and *Pcdh15* (**F**). Right, normalized gene expression values after the insertion sites of *Abcg2* (**C**), *Rasa1* (**E**), and *Pcdh15* (**G**) in all *SB*-induced tumors with and without insertions in the respective genes. *P* values were calculated using a Mann–Whitney *U* test, as implemented in IM-Fusion. **H,** Schematic overview of the *in vitro* competition assay performed with WESB-*Fgfr2* cells transfected with modified pX330 vectors containing sgRNAs targeting *Rasa1* (sg*Rasa1*) or a nontargeting sgRNA (sgNT). **I,** Competition assay of WESB-*Fgfr2*-sgNT and WESB-*Fgfr2*-sg*Rasa1* cells mixed in a 1:1 ratio at day 0. After 7, 10, and 12 days of vehicle or AZD4547-treatment (2 μmol/L), the allele distributions of the polyclonal populations were quantified by the percentage of frameshift mutations in *Rasa1* using the TIDE algorithm (29). The percentages of gene modifications are mean ± SD of at least four replicates.
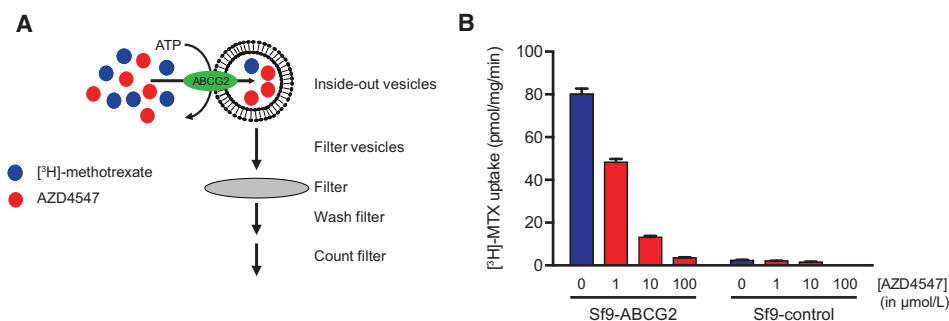
Figure 4.
AZD4547 is a substrate for ABCG2. **A,** Schematic overview of the vesicular transport assay. Control or ABCG2-containing inside-out membrane vesicles were incubated with [^{3}H]-MTX (blue) and increasing concentrations of AZD4547 (red) in the presence or absence of ATP. After 10 minutes incubation, the membrane vesicles were captured using rapid filtration and the filters were washed to eliminate the excess of [^{3}H]-MTX that was not transported into the vesicles. The retained radioactivity inside the membrane vesicles was measured using liquid scintillation counting. **B,** Inhibition of ABCG2-mediated [^{3}H]-MTX transport by increasing concentrations of AZD4547 (red). Values are corrected for transport in the absence of ATP. Data are mean ± SD of three independent experiments, which were each performed in triplicate.

ABCG2 (21). Furthermore, these MEFs lack both P-glycoprotein (P-gp, encoded by *Abcb1a* and *Abcb1b*), and the multidrug resistance-associated protein 1 (MRP1, encoded by *Abcc1*), allowing us to exclude confounding influences of these other drug efflux transporters. To test for drug sensitivity, MEF3.8 cells were transduced with an empty retroviral expression vector (MEF3.8-EV) or a vector containing *Abcg2* (MEF3.8-ABCG2) and subsequently exposed to increasing concentrations of AZD4547 in long-term clonogenic assays (Fig. 5A). Compared with MEF3.8 cells, MEF3.8-ABCG2 cells were able to survive higher concentrations of AZD4547 (Fig. 5B and C), indicating that increased ABCG2 expression reduces the efficacy of AZD4547.

To confirm that increased expression of ABCG2 also reduces the sensitivity of treatment-naive WESB-*Fgfr2* cells to AZD4547, we transduced these cells with an empty retroviral expression vector (WESB-*Fgfr2*-EV) or a vector containing *Abcg2* (WESB-*Fgfr2*-ABCG2) and treated the transduced cells with AZD4547. Short-term treatment of WESB-*Fgfr2*-EV cells with AZD4547 resulted in decreased phosphorylation of FGFR, FRS2α, and ERK1/2, whereas the phosphorylation levels of these proteins were less affected in AZD4547-treated WESB-*Fgfr2*-ABCG2 cells (Fig. 5D).

To test the effect of ABCG2 overexpression on the responsiveness of established tumors to AZD4547, we injected WESB-*Fgfr2*-EV and WESB-*Fgfr2*-ABCG2 cells into the mammary glands of immunocompromised NMRI-nude mice and these animals were treated with either vehicle or AZD4547 (12.5 mg/kg/day) daily for 30 days when the tumors reached the size of 62.5 mm^3. Interestingly, the NMRI-nude mice did not show tumor regression upon treatment with AZD4547, in contrast to the previously used FVB syngeneic animals (Supplementary Fig. S2B), suggesting that an intact immune system might enhance the therapeutic efficacy of AZD4547. Nonetheless, mice with WESB-*Fgfr2*-EV tumors did show stable disease, whereas WESB-*Fgfr2*-ABCG2 tumors progressed during treatment (Fig. 5E–G). These results show that increased ABCG2 expression also reduces the sensitivity of FGFR2-activated tumors to AZD4547 *in vivo*, confirming that upregulation of this drug efflux transporter can drive resistance to AZD4547.

Discussion

In this work, we performed an *SB*-based insertional mutagenesis screen in a mouse model of ILC to identify genes that are involved in the development of resistance to FGFR-targeting therapies. As a starting point for this screen, we used *SB*-induced mILCs, in which we previously identified *Fgfr2* as the most frequently mutated candidate gene (19). By orthotopically transplanting an *SB*-induced mILC with activated FGFR signaling into multiple recipient mice, we showed that treatment with the FGFR inhibitor AZD4547 initially results in tumor regression and provides long-term tumor control, but eventually results in acquired treatment resistance. Our mutational analysis of the AZD4547-resistant tumors identified several potential resistance mechanisms, including secondary mutations in FGFR2, inactivation of RASA1, a negative regulator of RAS signaling, and overexpression of MET and the drug-efflux transporter ABCG2. Together, these mechanisms explain acquired resistance to AZD4547 in (21 of 27) tumors (Fig. 6A). Resistance mechanisms in the remaining six tumors remain to be identified.

In line with previous studies in a mouse model of melanoma (30) and *Arf*$^{-/-}$ mice (31), we show that transposon mutagenesis in mice cannot only be used to identify candidate cancer genes, but is also an effective strategy to identify genes involved in *in vivo* drug resistance. In our mutational analysis of the AZD4547-resistant tumors, we exploited the constitutive activity of the *SB*-mediated insertional mutagenesis system in *SB*-induced mILCs to identify potential resistance mechanisms in an unbiased, genome-wide fashion. This allowed us to identify two resistance mechanisms (activation of ABCG2 and inactivation of RASA1), which might not have been identified without *SB* mutagenesis. However, resistance mechanisms that involve specific amino acid substitutions may not be uncovered by transposon mutagenesis, but only arise from spontaneous mutations. A comprehensive characterization of the various mechanisms of resistance to targeted anticancer therapeutics may therefore require a multipronged approach, combining transposon mutagenesis with other sequencing modalities to identify spontaneous mutations and/or transcriptional changes that may be driving resistance. Given enough sequencing depth, RNA-sequencing based approaches for identifying transposon insertions may be

Kas et al.
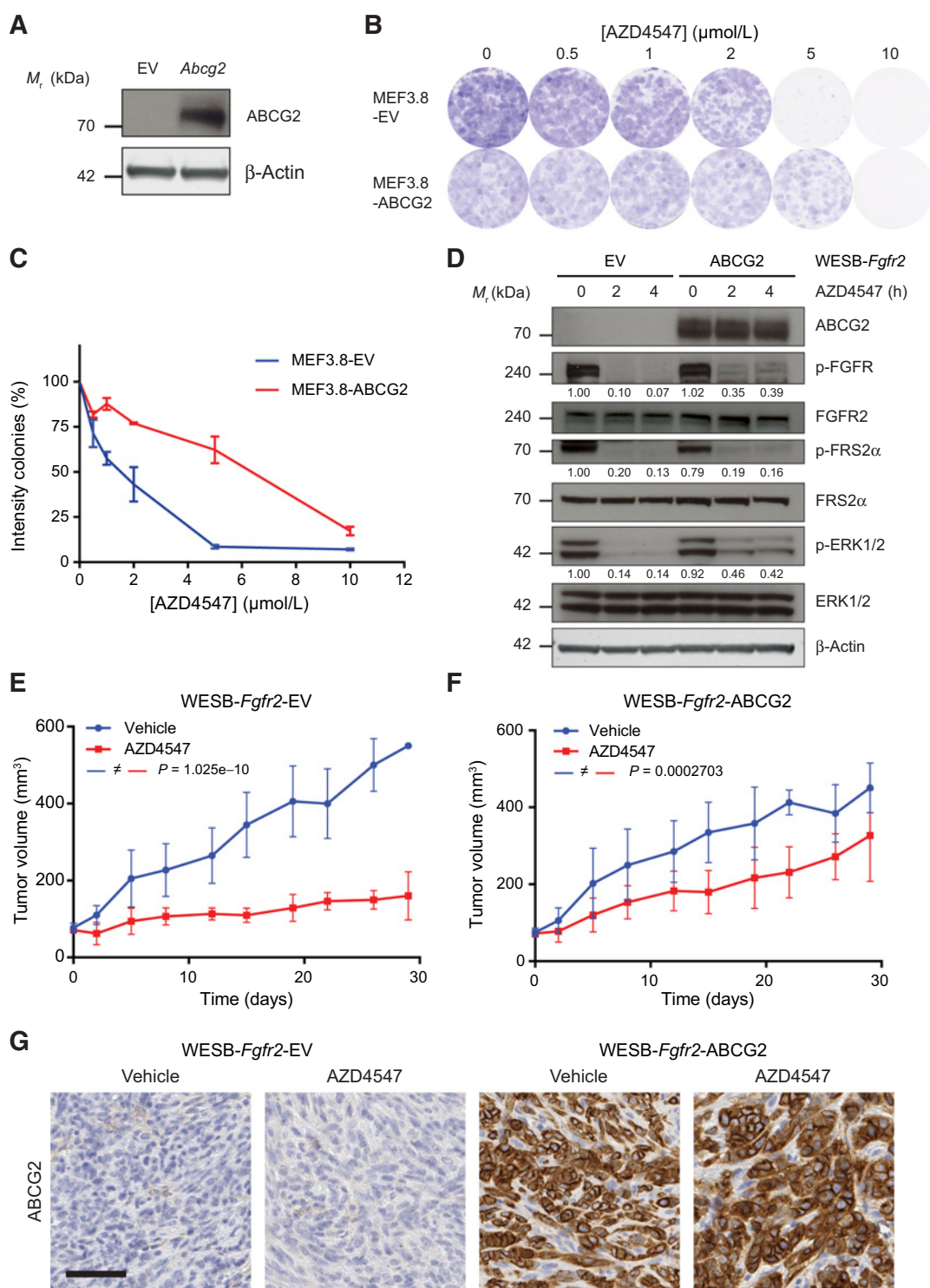
Figure 5.
ABCG2 reduces sensitivity to AZD4547 *in vitro* and *in vivo*. **A,** Representative immunoblot ($n = 3$) for the expression of ABCG2 in MEF3.8-EV and MEF3.8-ABCG2 cells. β-Actin was used as a loading control. **B** and **C,** Representative images (**B**) and quantification (**C**) of the clonogenic assays (11 days after seeding the cells) of MEF3.8 cells treated with increasing concentrations of AZD4547. Data are mean ± SD of three independent experiments. **D,** Representative immunoblot ($n = 3$) showing the effect of short-term AZD4547 treatment (100 nmol/L) in WESB-*Fgfr2* cells with and without ABCG2 expression. β-actin was used as a loading control. **E** and **F,** Tumor growth kinetics of WESB-*Fgfr2*-EV (**E**) and WESB-*Fgfr2*-ABCG2 (**F**) cells in NMRI-nude female mice under vehicle (blue) or AZD4547 (red) treatment (for 30 consecutive days). Datapoints are mean ± SD and *P* values were calculated using mixed linear models (details are described in the Supplementary Data). Vehicle-treated WESB-*Fgfr2*-EV versus WESB-*Fgfr2*-ABCG2 tumors, $P = 0.5511$, not significant; AZD4547-treated WESB-*Fgfr2*-EV versus WESB-*Fgfr2*-ABCG2 tumors, $P = 3.983e−05$. **G,** IHC detection of ABCG2 in sections of WESB-*Fgfr2*-EV and WESB-*Fgfr2*-ABCG2 tumors. Scale bar, 50 μm.

Figure 6.
Schematic overview of the resistance mechanisms in AZD4547-resistant tumors identified in this study. **A,** Overview of the genetic alterations and gene expression changes in the respective genes identified in the AZD4547-resistant tumors. Red bars, amplification of the respective gene. Blue and red triangles indicate insertions in sense or antisense orientation relative to the gene, respectively. Bars with a red outline indicate the upregulation of the respective genes. Green and black squares represent missense mutations in the IgIII-like domain or the tyrosine kinase domain of FGFR2, respectively. **B,** Schematic representation of the identified resistance mechanisms in the FGFR signaling pathway. Activating and inactivating events resulting in resistance to AZD4547 are depicted in green and red, respectively.
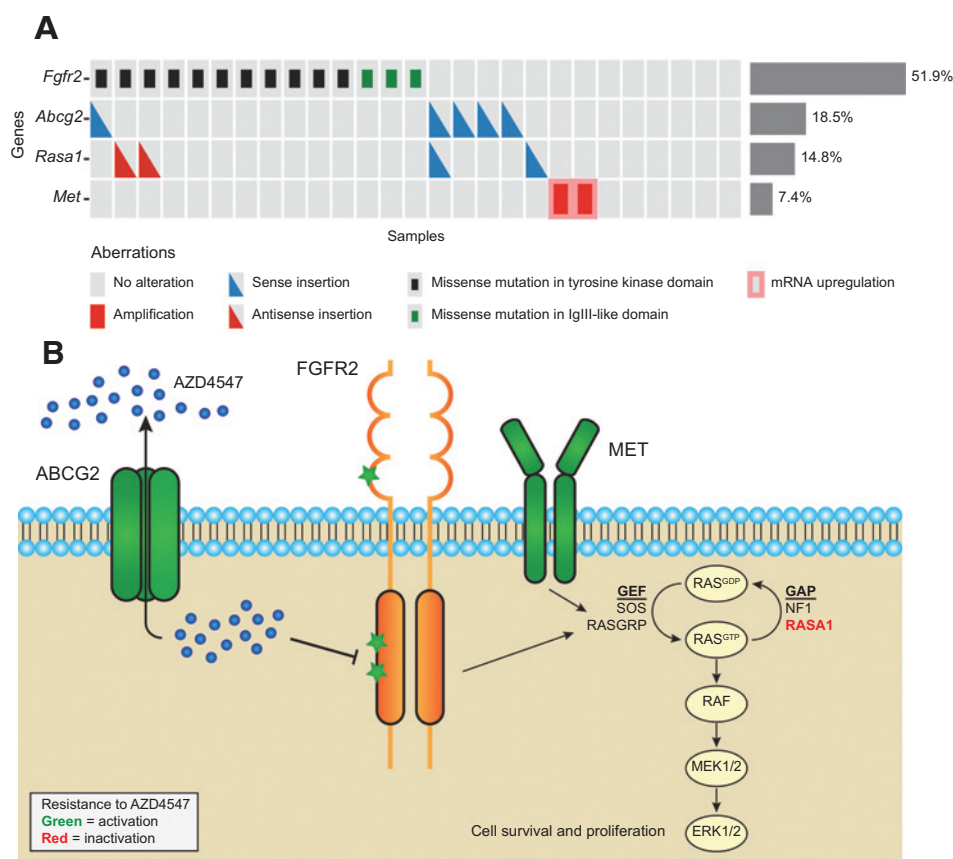
able to provide the most comprehensive analysis from a single dataset (26, 32), by allowing detection of transposon insertions, mutations, gene-fusions, and transcriptional changes in RNA-sequencing data. However, targeted DNA-sequencing approaches (as we have used here to detect *SB* transposon insertions) are likely to yield more detailed detection of insertions and/or mutations with a low frequency, by effectively providing deeper sequencing at a lower cost.

The diverse spectrum of identified resistance mechanisms illustrates the major challenge that (intra-) tumor heterogeneity poses for the prevention of therapy resistance, as we observe multiple resistance mechanisms arising from and within a single (donor) tumor. All of the identified mechanisms center on reactivation of the canonical MAPK–ERK signaling pathway, suggesting that this is a dominant mechanism for overcoming vulnerability to FGFR inhibition (Fig. 6B). Reactivation of MAPK–ERK signaling has also been identified as a predominant resistance mechanism to EGFR inhibitors (33). In our analysis of AZD4547-resistant tumors, we observed recurrent alterations in several components of the MAP–ERK pathway, including secondary mutations in FGFR2, overexpression of the MET receptor and inactivation of RASA1. MET overexpression can induce resistance by driving reactivation of signaling pathways downstream of FGFR2, as has previously been shown in the context of FGFR and other RTK inhibitors (2, 14, 15, 34). Also loss of RASA1, which is a negative regulator of RAS, may cause resistance to FGFR inhibition via reactivation of the MAPK–ERK pathway (35).

Our analysis of the secondary mutations in FGFR2 showed that the majority of these mutations occurred in the tyrosine kinase domain, suggesting that they mainly provide resistance by preventing the inhibitor from binding to the ATP-binding pocket and thereby reactivating the FGFR signaling pathway. This finding agrees with previous studies with other FGFR inhibitors, which identified polyclonal secondary FGFR mutations (including gatekeeper mutations) as a main resistance mechanism to FGFR-targeting treatments (10–12). Our observations are further supported by studies with other RTK inhibitors, which also describe secondary mutations in the receptor as one of the main resistance mechanisms to tyrosine kinase inhibitors (34).

Our validation of the drug efflux transporter *Abcg2* showed that increased ABCG2 expression can induce resistance by reducing the concentration of AZD4547 within tumor cells, which results in decreased inhibition of FGFR and reactivation of the FGFR signaling pathway. In patients, overexpression of the drug efflux pump MDR1 (encoded by *ABCB1*) has been observed in chemotherapy-resistant ovarian cancer (36). Our results suggest that drug efflux transporters such as ABCG2 cannot only drive therapy resistance in hematologic malignancies (37), but may also have similar effects on therapy efficacy in solid tumors.

Recent approaches have aimed to overcome resistance to FGFR-targeting therapies either by combining multiple existing RTK inhibitors (14, 15), or by designing irreversibly binding inhibitors such as FIIN-2, FIIN-3, and PRN1371 (38, 39), which cannot be disrupted as easily by secondary mutations in the receptor. However, our results suggest that combining FGFR and MEK/ERK inhibitors might be a more effective strategy, as this prevents reactivation of MAPK–ERK signaling. In addition, to avoid resistance resulting from drug efflux transporters, novel inhibitors

should be specifically designed to be poor substrates for common transporters. Alternatively, CRISPR/Cas9 genetic screens could be used to identify synthetic lethal interactions with FGFR inhibitors in the context of FGFR inhibitor-resistant tumors to design rational and more effective combination therapies to overcome drug resistance (40).

In summary, *SB* insertional mutagenesis in mice is an effective tool to identify mechanisms of drug resistance. A comprehensive analysis of AZD4547-resistant mILCs, in which *SB*-based mutagenesis is combined with targeted DNA- and RNA-sequencing, allowed us to explain the mechanism of resistance in 78% of the resistant tumors, of which all converged to the reactivation of the canonical MAPK–ERK signaling cascade. Altogether, our findings suggest that FGFR-targeting drugs might be improved by designing FGFR inhibitors that are poor substrates of drug efflux transporters and irreversibly bind to the ATP-binding pocket of the receptor to prevent secondary mutations in the tyrosine kinase domain. In addition, combining these novel FGFR inhibitors with MEK/ERK inhibitors might be an even more effective strategy for preventing resistance to FGFR-targeted therapies.

Disclosure of Potential Conflicts of Interest

C. Phillips and P.D. Smith have ownership interest (including patents) in AstraZeneca PLC. L.F.A. Wessels reports receiving a commercial research grant from Genmab. No potential conflicts of interest were disclosed by the other authors.

Authors' Contributions

Conception and design: S.M. Kas, J.R. de Ruiter, J. Jonkers
Development of methodology: S.M. Kas, J.R. de Ruiter, K. Schipper, L. Bombardelli, A. Berns, J. Jonkers
Acquisition of data (provided animals, acquired and managed patients, provided facilities, etc.): S.M. Kas,, K. Schipper, A.P. Drenth, R. de Korte-Grimmerink, S. Mahakena, K. van de Wetering,

Acknowledgments

References

1. Ornitz DM, Itoh N. The fibroblast growth factor signaling pathway. Wiley Interdiscip Rev Dev Biol 2015;4:215–66.
2. Babina IS, Turner NC. Advances and challenges in targeting FGFR signalling in cancer. Nat Rev Cancer 2017;17:318–32.
3. Porta R, Borea R, Coelho A, Khan S, Araújo A, Reclusa P, et al. FGFR a promising druggable target in cancer: molecular biology and new drugs. Crit Rev Oncol Hematol 2017;113:256–67.
4. Chae YK, Ranganath K, Hammerman PS, Vaklavas C, Mohindra N, Kalyan A, et al. Inhibition of the fibroblast growth factor receptor (FGFR) pathway: the current landscape and barriers to clinical application. Oncotarget 2017;8:16052–74.
5. André F, Bachelot T, Campone M, Dalenc F, Perez-Garcia JM, Hurvitz SA, et al. Targeting FGFR with dovitinib (TKI258): preclinical and clinical data in breast cancer. Clin Cancer Res 2013;19: 3693–702.
6. Nogova L, Sequist LV, Perez Garcia JM, Andre F, Delord J-P, Hidalgo M, et al. Evaluation of BGJ398, a fibroblast growth factor receptor 1-3 kinase inhibitor, in patients with advanced solid tumors harboring genetic alterations in fibroblast growth factor receptors: results of a global phase I, dose-escalation and dose-expansion study. J Clin Oncol 2017;35:157–65.
7. Tabernero J, Bahleda R, Dienstmann R, Infante JR, Mita A, Italiano A, et al. Phase I Dose-Escalation Study of JNJ-42756493, an oral pan-fibroblast growth factor receptor inhibitor, in patients with advanced solid tumors. J Clin Oncol 2015;33:3401–8.
8. Javle M, Lowery M, Shroff RT, Weiss KH, Springfeld C, Borad MJ, et al. Phase II study of BGJ398 in patients with FGFR-altered advanced cholangiocarcinoma. J Clin Oncol 2017;JCO2017755009.
9. Paik PK, Shen R, Berger MF, Ferry D, Soria J-C, Mathewson A, et al. A Phase Ib open-label multicenter study of AZD4547 in patients with advanced squamous cell lung cancers. Clin Cancer Res 2017;23:5366–73.
10. Goyal L, Saha SK, Liu LY, Siravegna G, Leshchiner I, Ahronian LG, et al. Polyclonal secondary FGFR2 mutations drive acquired resistance to FGFR inhibition in patients with FGFR2 fusion–positive cholangiocarcinoma. Cancer Discov 2017;7:252–63.
11. Chell V, Balmanno K, Little AS, Wilson M, Andrews S, Blockley L, et al. Tumour cell responses to new fibroblast growth factor receptor tyrosine kinase inhibitors and identification of a gatekeeper mutation in FGFR3 as a mechanism of acquired resistance. Oncogene 2013; 32:3059–70.
12. Byron SA, Chen H, Wortmann A, Loch D, Gartside MG, Dehkhoda F, et al. The N550K/H mutations in FGFR2 confer differential resistance to PD173074, dovitinib, and ponatinib ATP-competitive inhibitors. Neoplasia N Y N 2013;15:975–88.
13. Herrera-Abreu MT, Pearson A, Campbell J, Shnyder SD, Knowles MA, Ashworth A, et al. Parallel RNA interference screens identify EGFR activation as an escape mechanism in FGFR3-mutant cancer. Cancer Discov 2013;3:1058–71.
14. Kim S-M, Kim H, Yun MR, Kang HN, Pyo K-H, Park HJ, et al. Activation of the Met kinase confers acquired drug resistance in FGFR-targeted lung cancer therapy. Oncogenesis 2016;5:e241.
15. Chang J, Wang S, Zhang Z, Liu X, Wu Z, Geng R, et al. Multiple receptor tyrosine kinase activation attenuates therapeutic efficacy of the fibroblast growth factor receptor 2 inhibitor AZD4547 in FGFR2 amplified gastric cancer. Oncotarget 2015;6:2009–22.

16. Wang J, Mikse O, Liao RG, Li Y, Tan L, Janne PA, et al. Ligand-associated ERBB2/3 activation confers acquired resistance to FGFR inhibition in FGFR3-dependent cancer cells. Oncogene 2015;34:2167–77.

17. Wilson TR, Fridlyand J, Yan Y, Penuel E, Burton L, Chan E, et al. Widespread potential for growth-factor-driven resistance to anticancer kinase inhibitors. Nature 2012;487:505–9.

18. Harbinski F, Craig VJ, Sanghavi S, Jeffery D, Liu L, Sheppard KA, et al. Rescue screens with secreted proteins reveal compensatory potential of receptor tyrosine kinases in driving cancer growth. Cancer Discov 2012;2:948–59.

19. Kas SM, de Ruiter JR, Schipper K, Annunziato S, Schut E, Klarenbeek S, et al. Insertional mutagenesis identifies drivers of a novel oncogenic pathway in invasive lobular breast carcinoma. Nat Genet 2017;49:1219–30.

20. Doornebal CW, Klarenbeek S, Braumuller TM, Klijn CN, Ciampricotti M, Hau C-S, et al. A preclinical mouse model of invasive lobular breast cancer metastasis. Cancer Res. AACR; 2013;73:353–63.

21. Allen JD, Jackson SC, Schinkel AH. A mutation hot spot in the Bcrp1 (Abcg2) multidrug transporter in mouse cell lines selected for Doxorubicin resistance. Cancer Res 2002;62:2294–9.

22. van de Wetering K, Sapthu S. ABCG2 functions as a general phytoestrogen sulfate transporter in vivo. FASEB J 2012;26:4014–24.

23. van de Wetering K, Burkon A, Feddema W, Bot A, de Jonge H, Somoza V, et al. Intestinal breast cancer resistance protein (BCRP)/Bcrp1 and multi-drug resistance protein 3 (MRP3)/Mrp3 are involved in the pharmacokinetics of resveratrol. Mol Pharmacol 2009;75:876–85.

24. Stern DL. Tagmentation-based mapping (TagMap) of mobile DNA genomic insertion sites bioRxiv 2017. doi: https://doi.org/10.1101/037762.

25. Pettersen EF, Goddard TD, Huang CC, Couch GS, Greenblatt DM, Meng EC, et al. UCSF Chimera—a visualization system for exploratory research and analysis. J Comput Chem 2004;25:1605–12.

26. de Ruiter JR, Kas SM, Schut E, Adams DJ, Koudijs MJ, Wessels LFA, et al. Identifying transposon insertions and their effects from RNA-sequencing data. Nucleic Acids Res 2017;45:7064–77.

27. Wu Y-M, Su F, Kalyana-Sundaram S, Khazanov N, Ateeq B, Cao X, et al. Identification of targetable FGFR gene fusions in diverse cancers. Cancer Discov 2013;3:636–47.

28. de Ronde JJ, Rigaill G, Rottenberg S, Rodenhuis S, Wessels LFA. Identifying subgroup markers in heterogeneous populations. Nucleic Acids Res 2013;41:e200.

29. Brinkman EK, Chen T, Amendola M, van Steensel B. Easy quantitative assessment of genome editing by sequence trace decomposition. Nucleic Acids Res 2014;42:e168.

30. Perna D, Karreth FA, Rust AG, Perez-Mancera PA, Rashid M, Iorio F, et al. BRAF inhibitor resistance mediated by the AKT pathway in an oncogenic BRAF mouse melanoma model. Proc Natl Acad Sci U S A 2015;112:E536–545.

31. Chapeau EA, Gembarska A, Durand EY, Mandon E, Estadieu C, Romanet V, et al. Resistance mechanisms to TP53-MDM2 inhibition identified by in vivo piggyBac transposon mutagenesis screen in an Arf(-/-) mouse model. Proc Natl Acad Sci U S A 2017;114:3151–6.

32. Temiz NA, Moriarity BS, Wolf NK, Riordan JD, Dupuy AJ, Largaespada DA, et al. RNA sequencing of Sleeping Beauty transposon-induced tumors detects transposon-RNA fusions in forward genetic cancer screens. Genome Res 2016;26:119–29.

33. Rotow J, Bivona TG. Understanding and targeting resistance mechanisms in NSCLC. Nat Rev Cancer 2017;17:637–58.

34. Niederst MJ, Engelman JA. Bypass mechanisms of resistance to receptor tyrosine kinase inhibition in lung cancer. Sci Signal 2013;6:re6.

35. Hayashi T, Desmeules P, Smith RS, Drilon A, Somwar R, Ladanyi M. RASA1 and NF1 are preferentially co-mutated and define a distinct genetic subset of smoking-associated non-small cell lung carcinomas sensitive to MEK inhibition. Clin Cancer Res 2018;24:1436–47.

36. Patch A-M, Christie EL, Etemadmoghadam D, Garsed DW, George J, Fereday S, et al. Whole-genome characterization of chemoresistant ovarian cancer. Nature 2015;521:489–94.

37. Natarajan K, Xie Y, Baer MR, Ross DD. Role of breast cancer resistance protein (BCRP/ABCG2) in cancer drug resistance. Biochem Pharmacol 2012;83:1084–103.

38. Tan L, Wang J, Tanizaki J, Huang Z, Aref AR, Rusan M, et al. Development of covalent inhibitors that can overcome resistance to first-generation FGFR kinase inhibitors. Proc Natl Acad Sci U S A 2014;111:E4869–4877.

39. Venetsanakos E, Brameld KA, Phan VT, Verner E, Owens TD, Xing Y, et al. The irreversible covalent fibroblast growth factor receptor inhibitor PRN1371 exhibits sustained inhibition of FGFR after Drug Clearance. Mol Cancer Ther 2017;16:2668–76.

40. Brunen D, Bernards R. Drug therapy: Exploiting synthetic lethality to improve cancer therapy. Nat Rev Clin Oncol 2017;14:331–2.

Cancer Research

AACR American Association for Cancer Research

Transcriptomics and Transposon Mutagenesis Identify Multiple Mechanisms of Resistance to the FGFR Inhibitor AZD4547

Sjors M. Kas, Julian R. de Ruiter, Koen Schipper, et al.

Updated version	Access the most recent version of this article at: doi:10.1158/0008-5472.CAN-18-0757
Supplementary Material	Access the most recent supplemental material at: http://cancerres.aacrjournals.org/content/suppl/2018/08/16/0008-5472.CAN-18-0757.DC1

Cited articles	This article cites 38 articles, 16 of which you can access for free at: http://cancerres.aacrjournals.org/content/78/19/5668.full#ref-list-1

E-mail alerts	Sign up to receive free email-alerts related to this article or journal.
Reprints and Subscriptions	To order reprints of this article or to subscribe to the journal, contact the AACR Publications Department at pubs@aacr.org.
Permissions	To request permission to re-use all or part of this article, use this link http://cancerres.aacrjournals.org/content/78/19/5668. Click on "Request Permissions" which will take you to the Copyright Clearance Center's (CCC) Rightslink site.